Nanoscale

ROYAL SOCIETY OF CHEMISTRY

MINIREVIEW

View Article Online
View Journal | View Issue

Cite this: *Nanoscale*, 2023, **15**, 2541

Chiral inorganic nanomaterials for biological applications

Fang Wang,†[a] Xiaoyong Yue,†[a] Qi Ding,[a] Hengwei Lin,[a] Chuanlai Xu[b] and Si Li*[a]

Chiral nanomaterials in biology play indispensable roles in maintaining numerous physiological processes, such as signaling, site-specific catalysis, transport, protection, and synthesis. Like natural chiral nanomaterials, chiral inorganic nanomaterials can also be established with similar size, charge, surface properties, and morphology. However, chiral inorganic nanomaterials usually exhibit extraordinary properties that are different from those of organic materials, such as high *g*-factor values, broad distribution range, and symmetrical mirror configurations. Because of these unique characteristics, there is great potential for application in the fields of biosensing, drug delivery, early diagnosis, bio-imaging, and disease therapy. Related research is summarized and discussed in this review to showcase the bio-functions and bio-applications of chiral inorganic nanomaterials, including the construction methods, classification and properties, and biological applications of chiral inorganic nanomaterials. Moreover, the deficiencies in existing studies are noted, and future development is prospected. This review will provide helpful guidance for constructing chiral inorganic nanomaterials with specific bio-functions for problem solving in living systems.

Received 13th October 2022,
Accepted 2nd January 2023

DOI: 10.1039/d2nr05689e

rsc.li/nanoscale

[a]*International Joint Research Center for Photo-responsive Molecules and Materials, School of Chemical and Material Engineering, Jiangnan University, Wuxi, Jiangsu, 214122, People's Republic of China. E-mail: sili@jiangnan.edu.cn*
[b]*State Key Lab of Food Science and Technology, International Joint Research Laboratory for Biointerface and Biodetection, School of Food Science and Technology, Jiangnan University, Wuxi, Jiangsu, 214122, People's Republic of China*
†These authors contributed equally to this paper.

Si Li

Dr Si Li is an associate professor in the Department of Chemical and Material Engineering at Jiangnan University in China. She studied at Michigan University during 2016–2018 as a visiting student and received her Ph.D. degree from Jiangnan University in 2018. After working as a postdoctoral research fellow at Jiangnan University, she started her independent academic career in 2021. Her research is focused on constructing chiral inorganic nanostructures, studying the relationships between chiral morphologies and bio-effects, and exploring specific applications in biological systems.

1. Introduction

Chiral enantiomers denoted by the prefix *L*/*D*(*S*/*R*) are usually constructed with the same composition and functional groups and are generally mirror-symmetrical but never overlap.[1] Chiral substances widely exist in biological systems, including DNA, RNA, protein, and saccharide. These natural macromolecules or macromolecules with homochiral properties play indispensable roles in maintaining normal life activities. For example, because amino acids in living systems are usually formed in the L-form, and saccharides are generally presented in the D-form,[2] there is high selectivity of living systems toward chiral drugs.

Typically, only one configuration for chiral medicines exhibits pharmacological activity, while the enantiomer generally has no effect or toxicity. For example, L-dopamine can alleviate Parkinson's disease, whereas D-dopamine may cause mitochondrial deficiency and weight loss.[3,4] There has been considerable research on the applications of chiral enantiomers in biological and medical science due to their specific biological performances. However, the difficulties in extracting and storing chiral nanomaterials in biological systems largely limit their extensive application *in vitro* and *in vivo*.

Unlike natural chiral materials, inorganic materials within the nanoscale have high surface-to-volume ratios, specific optical/electrical/magnetic properties,[5] high structural stability, great endurance in harsh environments,[6] and excellent

versatility and flexibility in construction.[7] These properties endow the chirality of inorganic nanomaterials with new characteristics, such as high *g*-factor value, enantiomeric configuration, and bathochromic shift of the circular dichroism (CD) signal. Inspired by the unique properties of chirality, there is great potential for chiral inorganic nanomaterials in the fields of biocatalysis, biosensing, disease diagnosis, and treatment.[8,9]

In this review, classification and summaries describing the preparation, characterization, and application of chiral inorganic nanomaterials and their biological activities are provided for a thorough understanding of the biological development of chiral inorganic nanomaterials. The shortcomings of the present research, as well as future challenges, are briefly discussed.

2. Construction methods for chiral inorganic nanomaterials

Chiral nanomaterials are usually constructed using two primary methods: top-down and bottom-up strategies.[10] The top-down method is generally achieved by photolithography, which uses light to produce small particles with subtle patterns from the entire block. This method is primarily limited by its high requirements for equipment and instruments.[6] The bottom-up approach provides a convenient and versatile method to prepare chiral inorganic nanomaterials with excellent functional performances.[11]

2.1 Chiral ligand-mediated construction method

Among the numerous synthetic strategies to produce chiral inorganic nanomaterials, the chiral ligand-mediated construction method is one of the simplest, most efficient, and most convenient strategies, and is widely used to construct chiral nanomaterials with unique morphologies and specific functions. Chiral ligands, including amino acids, short peptides, and chiral derivatives, play unsubstituted roles in the chiral ligand-mediated construction method (Fig. 1).

According to the addition period for chiral ligands, chiral ligand-mediated construction can occur at the beginning of synthesis, during the midpoint of the synthetic process, and at post-modification after synthesis. At the beginning of synthesis, chiral ligands usually form chiral complexes with metal ions to guide the construction of inorganic cores.[12] Chiral enantiomers of organic ligands can lead to the distortion of the surficial crystal lattice, which would endow inorganic nanoparticles (NPs) with high chiral optical activity. For example, Yeom *et al.* synthesized Co_3O_4 NPs with a strong and symmetrical CD signal by adding L-/D-cysteine (Cys) at the beginning of synthesis.[13]

Magnetic fields can be used to modulate the transparency of Co_3O_4 NPs gel corresponding to the circularly polarized light (CPL) in the ultraviolet (UV) range, which should be pivotal knowledge regarding chirality and magnetism. Chiral graphene oxides prepared by Huang *et al.* were also obtained by adding L-/D-Cys at the beginning of synthesis,[14] and this useful method was applied for the chiral recognition of tartrates by voltammetry signal response. Using this method, Jiang *et al.* found that the bonding state between chiral ligands and WO_x NPs greatly affected the intensity and distribution of chiral signals,[15] and the construction of chiral WO_x NPs successfully regulated CD signals in the near-infrared range (NIR).

Many steps are usually required to incorporate chiral ligands into the medium of synthesis to construct chiral nanomaterials. Typically, asymmetric gold nanomaterials with strong chiral optical activities are constructed within two steps: first, gold nanocubes with high Miller index facets are synthesized as seeds, and then, chiral ligands such as Cys or glutathione (GSH) are modified on the high index facets of nanocubes to guide the regrowth for constructing chiral nanomaterials.[16–18]

In recent research, Wen *et al.* used gold nanorods (NRs) as seeds and L-$SeCys_2$ as a chiral inducer to construct chiral gold nanoarrows (NAs). With UV irradiation on L-$SeCys_2$, gold NAs were constructed with helical groove features and strong plasmonic CD signals.[19] This work may advance the design and construction of chiral plasmonic nanomaterials. Wan *et al.* synthesized helical grooved NAs by using L-/D-Cys to direct the helical growth orientation of NAs, and helical morphology and chiral optical activities were controlled by the concentration of chiral ligands. In addition, helical NAs can assemble into super-helical structures by using high concentrations of chiral ligands, and the chirality can be transcribed to achiral azobenzene as well.[20] The related studies can deepen our understanding of plasmon-chirality-coupled CD.

Except for the above two methods, chiral nanomaterials can be constructed through post-translational modification on synthesized NPs as well.[21,22] For example, Morales-Vidal *et al.* used L-Cys to modify the surface of achiral gold NPs to construct chiral gold NPs. They found that L-Cys preferred to bind to Au (321), which then induced an enantiomeric enrichment and chiral template effect.[23] Based on the post-modification method, Rodríguez-Zamora *et al.* studied the interaction between chiral molecules and inorganic surfaces, and demonstrated their effects on the chiral morphology of inorganic cores.[24] G. M. Li *et al.* found that the chirality of CdTe originated from the interaction between chiral ligands and quantum dots (QDs), which were linked together by the covalent bonding of –SH and surficial metal ions.[25]

Understanding the relationship between QD surfaces and chiral ligands can provide a useful perspective on the origin of chiral properties of semiconductor NPs. Kuznetsova *et al.* demonstrated that the concentration of chiral ligands and the bonding modes between chiral ligands and inorganic NPs significantly affected the chiral optical activities of CdSe/CdS QDs.[26]

2.2 Self-assembly method

Self-assembly is a powerful method that can be used to assemble various types of achiral or chiral building blocks into specific morphologies with strong chiral optical activities.[27,28] A soft or rigid chiral template can be used to guide the con-

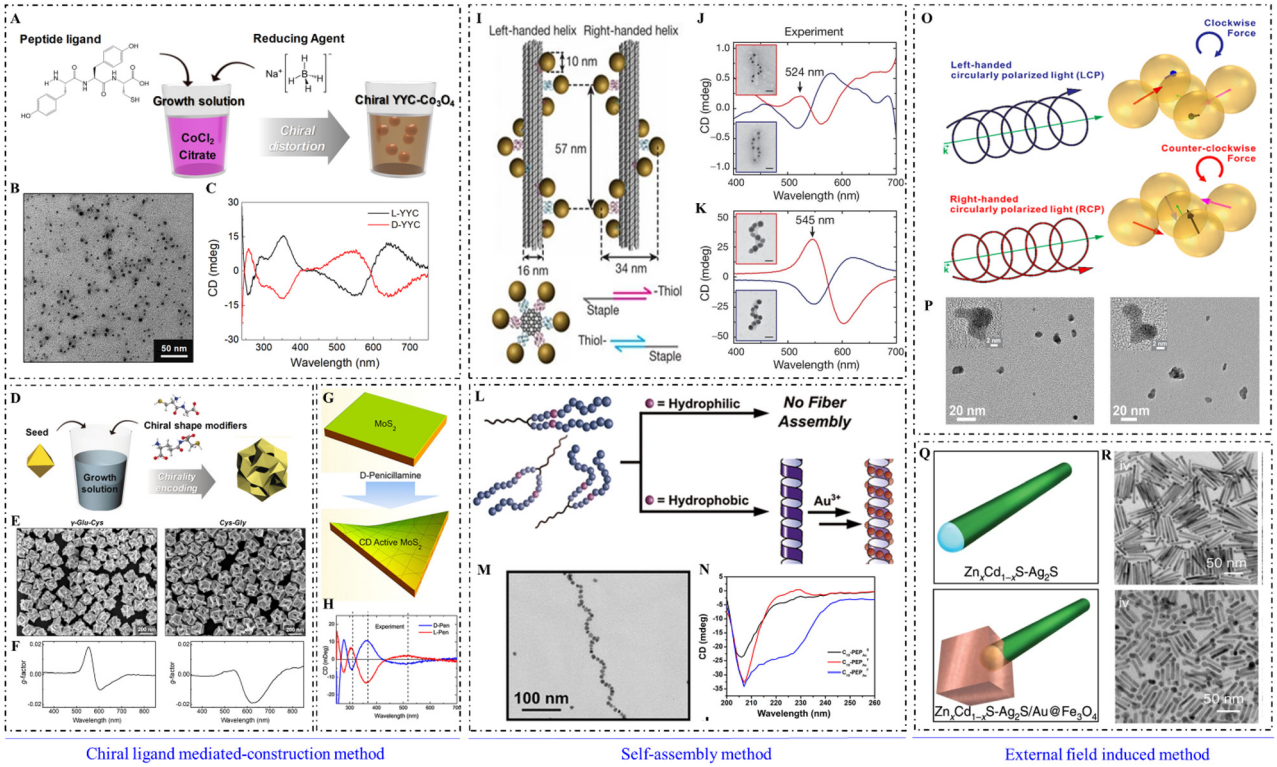

Fig. 1 Synthetic methods of chiral inorganic NPs. (A) Synthetic illustration of the formation of chiral cobalt oxide NPs by adding Tyr–Tyr–Cys at the beginning of synthesis. (B) Transmission electron microscopy (TEM) image of chiral cobalt oxide NPs. (C) CD spectra of chiral cobalt oxide NPs.[12] Reproduced from ref. 12 with permission from American Chemistry Society, copyright 2020. (D) Synthetic illustration of chiral gold NPs by adding dipeptide at the midpoint of synthesis. (E) Scanning electron microscope (SEM) images of chiral gold NPs. (F) Dissymmetric factor spectrum of chiral gold NPs.[18] Reproduced from ref. 18 with permission from Wiley, copyright 2020. (G) Schematic of the construction method for production of chiral MoS_2 sheets using a post-modification method. (H) CD spectra of L-/D-Pen-modified MoS_2 sheets.[22] Reproduced from ref. 22 with permission from American Chemistry Society, copyright 2018. (I) Schematic of DNA origami-mediated construction of gold nano-helices. CD spectra of left-handed (red lines) and right-handed (blue lines) helices composed of (J) 10 nm gold particles and (K) 16 nm gold particles.[32] Reproduced from ref. 32 with permission from Nature Publishing Group, copyright 2012. (L) Scheme of peptide conjugation-mediated assembly of gold NPs. (M) TEM image of gold nano-helices mediated by C_{14}-$(PEP_{Au}{}^{M\text{-}ox})_2{}^{F}$. (N) CD spectra of C_{10}-$PEP_{Au}{}^{X}$ assemblies.[33] Reproduced from ref. 33 with permission from the American Chemistry Society, copyright 2021. (O) Schematic of CPL-induced formation of chiral gold nanostructures. (P) High-resolution TEM images of gold nanostructures obtained with LCP (left) and RCP (right) illumination, respectively.[41] Reproduced from ref. 41 with permission from the American Chemistry Society, copyright 2019. (Q) Models of $Zn_xCd_{1-x}S$-Ag_2S (top) and $Zn_xCd_{1-x}S$-Ag_2S/Au@Fe_3O_4 (bottom) hetero NRs. (R) TEM images of $Zn_xCd_{1-x}S$-Ag_2S (x = 0.3) (top) and $Zn_{0.3}Cd_{0.7}S$-Ag_2S/Au@Fe_3O_4 (x = 0.3) (bottom).[44] Reproduced from ref. 44 with permission from Nature Publishing Group, copyright 2020.

struction of chiral inorganic nanostructures. Soft templates include chiral gels, liquid crystals, protein/peptide fibrils, or DNA origami.[29] The rigid template can be exemplified by chiral mesoporous silica.

Inorganic NPs usually assemble with chiral soft templates using noncovalent or covalent interactions,[30] and they can form into dimers, trimers, tetramers, helices, NRs, pyramids, and other complex morphologies with strong chiral optical activities. For example, silver or gold NPs can assemble into helical nanostructures using the DNA framework as a chiral template.[31,32] Gold nano-helixes can also be established by *in situ* reduction of Au^{3+} using peptide assemblies as chiral templates. It was found that the terminal structure of chiral gold NP superstructures could be changed by a subtle change in peptide sequences.[33] Gold NRs can also aggregate on protein fibers to form plasmonic structures with strong chiral signals in the NIR,[34] which was used to analyze the chiral origin as well as the single particle level structure. Cheng *et al.* used silica helices as chiral templates to guide the assembly of gold NPs, which formed nano-helixes with strong chiral signals.[35]

Complementary DNA sequences can be also used to construct chiral inorganic nanostructures. Zhu *et al.* achieved the chiral self-assembly of gold NPs based on the polymerase chain reaction (PCR) technique. Nevertheless, the high environmental requirement of enzymes largely limits the extensive application of PCR-based construction methods. If single-stranded DNA molecules were initially modified on the surface of inorganic NPs, inorganic building blocks can also be assembled into specific morphologies by the complementary interactions of DNA sequences. Nanoassemblies such as gold and silver dimers, and homogeneous or heterogeneous nanopyramids can be constructed using single-stranded DNA sequences. Kuang *et al.* assembled four different NPs into the

L- and *D*-enantiomers of chiral pyramids using complementary DNA sequences, which exhibited symmetrical chiral signals in the visible range.[36] The simplicity of this construction method and the subsequent predictable chiral optical activities facilitate the future application of nanopyramid enantiomers.

Kumar *et al.* prepared chiral plasmonic NPs using quaternary alkylammonium halide micellar aggregates to assemble with anisotropic gold NRs. Helical plasmonic structures with strong chiral optical activities in the NIR and controllable morphologies were formed,[37] which provided a promising strategy for light management or chiral sensing. Cys-modified CdTe NPs can also be assembled into helical nanostructures with high anisotropy values by solvent-induced self-assembly, and the NIR chiral optical activities can be regulated by varying the pitch of semiconductor helices.[38]

2.3 External field-induced method

External fields with chiral properties also play crucial roles in endowing nanomaterials with chiral properties. CPL and magnetic fields are common for constructing chiral inorganic nanomaterials. The 'lock' ability of inorganic NPs toward the chirality of external fields provides a promising strategy to construct inorganic nanostructures with high chiral optical activities.

CPL, acting as a physical force, can drive the formation of chiral inorganic nanomaterials due to the chirality transfer from chiral photons to matter.[39] As exemplified by chiral gold NPs constructed by Tatsuma *et al.*, CPL with left/right-handedness was used to synthesize chiral plasmonic nanostructures. CPL can also create a distorted electric field and guide the regrowth of gold nanocubes from the corner by redox reactions.[40] Moreover, Kotov *et al.* used CPL to irradiate gold salt solutions to form gold nanostructures with chiral features. The asymmetric displacement of gold NPs in the dynamic assembly process was driven by the CPL.[41] Recently, H. Wang *et al.* used CPL to achieve site-selective chiral modulation. Cys was adsorbed on the high-index crystal face of gold NPs first and then irradiated with R-/L-CPL during the regrowth of gold NPs.[42] Chiral semiconductor nanomaterials can also be constructed by CPL irradiation. For example, achiral CdTe NPs can assemble into left- and right-handed twisted nanoribbons under the illumination of circularly polarized photons with spin-angular momentum (Fig. 2).[43]

Magnetic fields can also be used to construct chiral NPs. For example, external magnetic fields with certain angles can regulate the chiral optical activities of paramagnetic cobalt oxide NPs,[13] by which Fe_3O_4 NPs can grow on the surface of silver NPs with chiral properties.[44]

3. Categories and properties of chiral inorganic nanomaterials

Compositions confer excellent effects on the terminal functions of inorganic nanomaterials, which largely affect the biological application of inorganic nanomaterials. According to compositional differences, chiral inorganic nanomaterials can be classified into metal, semiconductor, ceramic, and compositive nanomaterials (Fig. 3).

3.1 Chiral plasmonic nanomaterials

Metal nanomaterials confer specific plasmonic effects, leading to unique optical properties. Metal nanomaterials with strong CD signals, high *g*-factor values, broad signal distribution range, specific morphologies, and multiple functional properties have been extensively constructed and displayed great application potential in biocatalysis, biosensing, disease diagnosis and treatment, and drug delivery due to their unique optical, thermal, electronic, magnetic, mechanical, and chemical properties.

Kumar *et al.* found that amyloid fibrils can be used as chiral templates by guiding the assembly of gold NRs using tip-to-tip alignments, and forming them into a three-dimensional (3D) helical NR structure. Moreover, bisignate CD signals in the NIR were observed at the longitudinal surface plasmon wavelength for the constructed helical NR structures according to the exciton coupling between two equal dipoles, while negligible interaction was observed between NRs and protein monomers. Taking advantage of this phenomenon, a new detection strategy for amyloid fibrils was constructed using plasmonic chirality.[45]

Zhang *et al.* found that bovine serum albumin (BSA) induced NR aggregation into chiral nanostructures with strong plasmonic CD signals due to the structural chirality of plasmonic aggregates and the strong coupling between chiral proteins and surface plasmons. Understanding the chirality origins of the BSA-induced construction of chiral NR aggregation can assist in identifying the chirality of single biomolecules.[46] Using the plasmonic coupling between Cys enantiomers and the plasmonic surface of DNA-driven shell–satellite gold assemblies, a new inorganic photodynamic therapy agent with intense plasmonic CD signals in the visible range was developed by Gao *et al.* that produced $^1O_2$ with a high quantum of 1.09 under the irradiation of CPL. This study provides a new method for the construction of diagnostic and therapeutic agents.[47]

By coating silver on the surface of DNA-functionalized gold NRs, Heuer-Jungemann *et al.* synthesized gold (core)–silver (shell) NRs with high chemical stability and excellent optical performance, which enabled chiral self-assembly on DNA origami. The silver surface of NRs gave rise to an obvious enhancement of plasmonic properties and led to a strong CD signal due to the synergistic effects of plasmonic coupling. This work provides an ideal candidate for plasmonic sensing of biological targets.[48]

Furthermore, Lan *et al.* used DNA origami to construct 3D chiral plasmonic nano-helixes. Upon the reconfiguration of DNA templates, the handedness of constructed nano-helixes can be reconfigured to the opposite. Moreover, the amplitude of the CD signal, the frequency of peak response, and the signature of chirality can also be switched.[49] C. Xu *et al.* used Cys enantiomer-modified gold NPs as building blocks to construct plasmonic nanoassemblies with reconfigurable morphologies and chiroptical activities. These types of chiral plasmonic

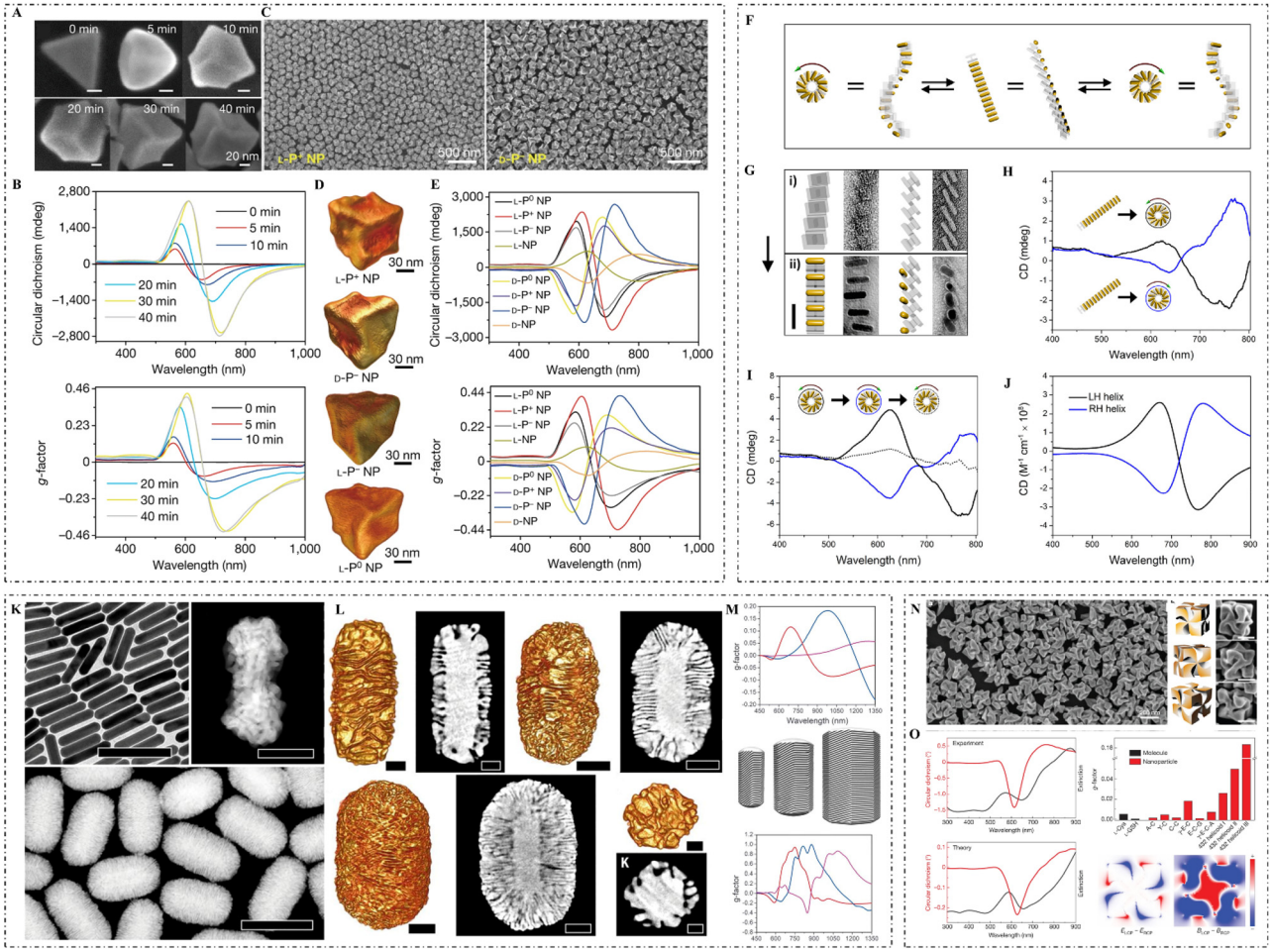

Fig. 2 (A) SEM images and (B) CD spectra and *g*-factor spectra of L-P$^+$ gold NPs synthesized under 0, 5, 10, 20, 30, and 40 min illumination. (C) SEM images of L-P$^+$ gold NPs (left) and D-P$^-$ gold NPs (right). (D) TEM tomography images of L-P$^+$, D-P$^-$, L-P$^-$, and L-P^0 gold NPs. (E) CD spectra (top) and *g*-factor spectra (bottom) of gold NPs synthesized under different light conditions in the presence of CYP dipeptides: L-P$^+$ NPs (under LCP illumination), D-P$^-$ NPs (under RCP illumination), D-P$^+$ NPs (under LCP illumination), L-P$^-$ NPs (under RCP illumination), L-P^0 NPs (under LP illumination), D-P^0 NPs (under LP illumination), L-NPs (without light illumination), and D-NPs (without light illumination).[51] Reproduced from ref. 51 with permission from Nature Publishing Group, copyright 2022. (F) Mechanistic illustration of the conversion of gold NR superstructures into two mirror-image states. (G) TEM images of DNA origami superstructures (top) and gold NR superstructures (bottom). (H) CD spectra of the two mirror-imaged states. (I) CD spectra of a full cycle conversion between the left-handed and right-handed superstructures. (J) Theoretically calculated CD spectra of a left-handed and a right-handed superstructure.[49] Reproduced from ref. 49 with permission from the American Chemistry Society, copyright 2018. (K) TEM image of gold NRs (top left), high magnification HAADF-STEM image of a chiral gold NR grown in (*R*)-BINOL (top right), and low magnification HAADF-STEM images of gold NRs obtained in the presence of (*R*)-BINAMINE (bottom). (L) HAADF-STEM and corresponding tomography reconstructions of gold NRs with sizes of 165 × 73 nm (top left two), 210 × 112 nm (top right two), and 270 × 175 nm (bottom left two), and low magnification STEM image and tomography reconstruction (bottom right) of NPs obtained in an (*R*)-BINAMINE/surfactant mixture. (M) Spectral evolution of the anisotropy factor (top) for chiral NRs with sizes of 165 × 73 nm (red), 210 × 112 nm (blue), and 270 × 175 nm (magenta), as well as models of chiral gold NRs (middle) with increasing particle size (from left to right) and calculated anisotropy factor spectra (bottom).[37] Reproduced from ref. 37 with permission from the American Association for the Advancement of Science, copyright 2020. (N) SEM image of 432 helicoid III NPs (left), three-dimensional models (middle) and corresponding SEM images (right) of 432 helicoid III oriented in various directions. (O) Experimental (top left) and theoretical (bottom left) CD and extinction spectra of 432 helicoid III, comparison of the dissymmetry *g*-factors of the synthesized helicoid structures and other NPs (top right), and the asymmetric responses of the electric and magnetic (bottom right: from left to right) fields under CPL.[17] Reproduced from ref. 17 with permission from Nature Publishing Group, copyright 2018.

nanostructures can induce a CPL-dependent force on the cellular skeleton and facilitate the differentiation of neural stem cells into neuronal phenotypes, which can be used for the alleviation of neurodegenerative diseases (Fig. 4).[50]

Lee *et al.* used a two-step growth method to construct chiral gold nanocrystals. They utilized gold nanocubes as the seed, and then modified the high-index crystal surfaces with amino acid enantiomers to guide the regrowth direction of the nanocrystals.[17] The gold NPs they synthesized displayed strong chiral plasmonic optical activities with a dissymmetry factor of 0.2. Furthermore, L. Xu *et al.* exploited gold nanotriangles as seeds and modified their high-index crystallographic surface

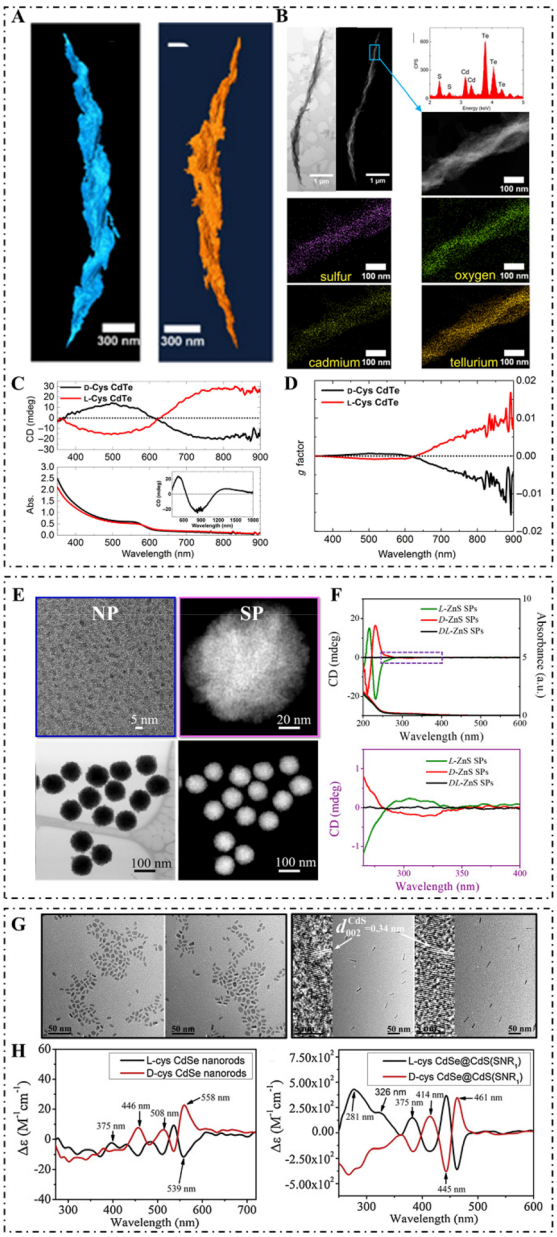

Fig. 3 (A) STEM tomography of the R-helix (left) and L-helix (right). (B) Bright-field STEM and HAADF-STEM images of the R-helix (top left: from left to right), STEM-EDX spectrum and HAADF-STEM image of the highlighted region (top right: from top to bottom), and elemental mapping of sulfur, oxygen, cadmium, and tellurium, respectively. (C) CD (top) and absorption (bottom) spectra of L-/D-Cys CdTe assemblies in water (inset shows the CD spectra of D-Cys CdTe assemblies in D_2O). (D) *g*-Factor spectra of L-/D-Cys CdTe assemblies.[52] Reproduced from ref. 52 with permission from the American Association for the Advancement of Science, copyright 2017. (E) TEM image of L-Pen-stabilized ZnS NPs (top left), magnified HAADF-STEM image of L-ZnS SPs (top right), and HAADF-STEM image and bright-field STEM image of L-ZnS SPs (bottom: from left to right). (F) CD and UV spectra (top) and enlarged CD spectra (bottom) of L-/D-/DL-ZnS SPs.[80] Reproduced from ref. 80 with permission from Nature Publishing Group, copyright 2019. (G) TEM of D-Cys CdSe NRs, L-Cys CdSe NRs, D-Cys CdSe@CdS NRs (SNR1), and L-Cys CdSe@CdS NRs (SNR1) (from left to right); the corresponding HRTEM is shown in the inset. (H) CD spectra of L-/D-Cys CdSe NRs (left) and L-/D-Cys CdSe@CdS NRs (right).[59] Reproduced from ref. 59 with permission from Elsevier, copyright 2019.

with amino acids or short peptides. Thus, the CPL used for the regrowth process resulted in a *g*-factor value as high as 0.4 for the final synthesized enantiomeric NPs.[51]

3.2 Chiral semiconductor nanomaterials

Semiconductor NPs possess excellent optical properties such as broad absorption and excitation, narrow and tunable emission peaks, and excellent photocatalytic ability. Chiral semiconductor nanomaterials have been widely applied in bioimaging, biosensing, disease diagnosis, and therapy, taking advantage of these characteristics.

In the field of chiral semiconductor nanomaterials, there has been wide interest in CdSe/CdS QDs synthesized with chiral ligands.[52] For example, Hao *et al.* developed L-/D-Cys-capped CdSe/CdS nanoplatelets (NPLs) with high CD and CPL signals. The effects of CdS shell thickness and shape variation on the CD and CPL activities were systematically demonstrated.[53] Moloney *et al.* reported a new microwave-based method for constructing chiral CdS, CdSe, CdTe, and ZnS QDs using chiral ligands.[54] This work demonstrated that the behavior, properties, and structure were strongly dependent on the chiral stabilizers and were affected by the synthetic procedures as well.

X. Wang *et al.* constructed chiral ultrathin CdSe NPLs based on the transfer from chiral ligands to achiral NPLs.[55] Recently, L-/D-Ag_2S QDs with intense fluorescence emission in the NIR-II spectral window and symmetrical CD signals in the UV region were prepared with chiral *N*-isobutyryl-Cys, which provided a new method for enhancing the targeting ability of nanoprobes by regulating their surface chirality.[56] Generally, the type of chiral ligand dramatically influences the chiral optical activity of semiconductor material.[25]

3.3 Chiral ceramic nanomaterials

The melting points for ceramic nanomaterials are higher, and they possess increased strength and hardness, and higher electrical and thermal conductivity. Due to the unique physical and chemical properties of ceramic nanomaterials, chirality is endowed with specific properties.[15]

For example, H. R. Li *et al.* used alanine derivatives as chiral ligands to synthesize twisted mesoporous silica rods that can be used as nanocarriers and loaded with ibuprofen.[57] According to Maqbool *et al.*, supra-assembled Fe_3O_4 magnetite NPs with enhanced chiral magneto-optical activity exhibited superparamagnetic properties under a weak magnetic field,[58] and were the same as chiral Co_3O_4 NPs.[13] The variety of chiral ligands also significantly affects the distribution range and intensity of chiral optical activity.[15]

3.4 Chiral compositive nanomaterials

Compositive nanomaterials can integrate optical, electrical, mechanical, electrochemical, thermal, and catalytic properties, and the functionalities of inorganic nanocomposites can be regulated and controlled by changing the composition of the nanomaterials. Many chiral inorganic nanocomposites with excellent bio-functions have been developed for problem solving in living systems.[59–61]

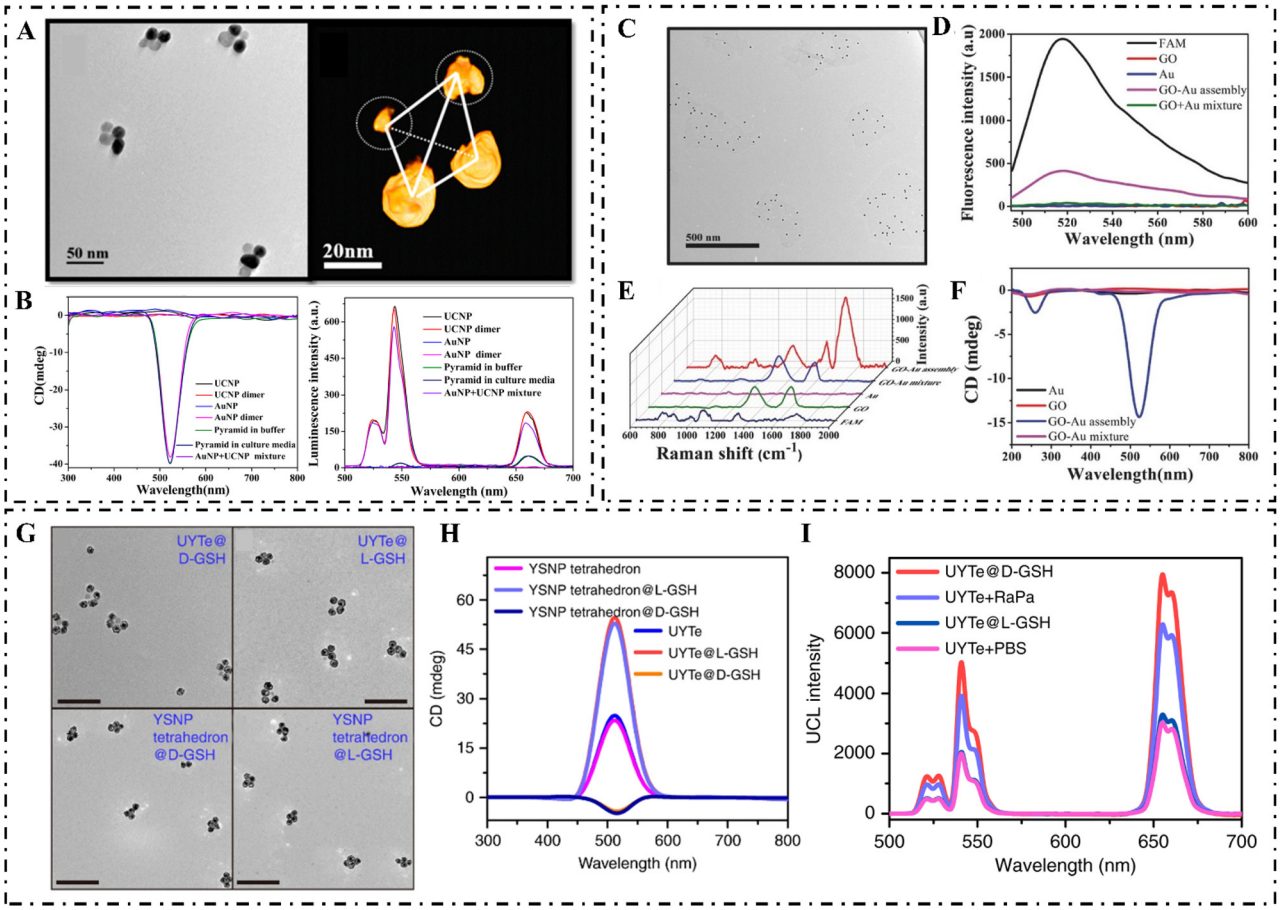

Fig. 4 (A) TEM images (left) and 3D reconstruction cryo-TEM tomography image (right) of pyramids assembled with gold NPs and UCNPs. (B) CD (left) and (right) luminescence spectra of gold NP, UCNP, gold NP-DNA, UCNP-DNA, gold NPs dimers, UCNP dimers, and gold NPs + UCNP mixture.[63] Reproduced from ref. 63 with permission from the American Chemistry Society, copyright 2016. (C) TEM image of GO–gold assemblies (probe Ep). (D) Fluorescence spectra of probe Ep. (E) SERS spectra (probe mR) and (F) CD spectra (probe Ep) of GO, gold, gold + GO mixture, and assemblies of GO and gold.[60] Reproduced from ref. 60 with permission from Wiley, copyright 2017. (G) TEM images of D-GSH and L-GSH-modified UYTE (top: from left to right), and D-GSH and L-GSH-modified YSNP tetrahedrons (bottom: from left to right). (H) The CD spectrum of L-/D-GSH-modified UYTe and YSNP tetrahedrons. (I) UCL intensity of MCF-7 cells after different treatments.[61] Reproduced from ref. 61 with permission from Nature Publishing Group, copyright 2018.

For example, MacLachlan *et al.* loaded a metal precursor into chiral mesoporous silica by a vacuum-assisted method, and Cu/Zn NPs or metal oxides were formed by high-temperature treatment and displayed a high surface area, thus facilitating their use as heterogeneous catalysts for click reactions.[62] S. Li *et al.* developed DNA-driven gold-upconversion nanopyramids that displayed strong upconversion luminescence and chiral plasmonic activities. The gold-upconversion nanopyramid was able to detect intracellular microRNAs in real-time with high selectivity and sensitivity.[63]

Nguyen *et al.* recently constructed gold (core)–silver (shell) NRs using a DNA origami-mediated self-assembly method, and they exhibited high sensitivity for the detection of viruses or antibodies.[48] In addition, Shao *et al.* used L-/D-Cys or phenylalanine (Phe) to synthesize Cu_2S (core)–CdSe (shell) NPs. By changing the chiral ligands and adjusting the thickness of the CdSe shells, it was possible to regulate the CD signal of Cu_2S (core)–CdSe (shell) NPs.[64] This study increased our understanding of the interaction between chiral ligands and inorganic core/shell semiconductor nanostructures. Yang *et al.* found that alloying gold on the surface of a palladium nano-helix largely improved the CD signal, which paved the way for biological sensing and catalysis.[65,66] Moreover, Cys-modified gold–silver nanotubes exhibited high chiroptical responses when subjected to strong localized electromagnetic fields.[67] Under a helical magnetic field, the chirality of silver (core)–Fe_3O_4 (shell) NPs can be regulated by changing the magnetic field in real-time.[68]

4. Biological applications

Because of the homochirality of living systems, nanomaterials with specific chiral configurations exhibit extraordinary advantages in biomedical fields due to their high cellular uptake efficiency, increased cellular stability, higher bio-selectivity,

and higher biocompatibility.[8,69] As for biological applications, it is necessary to consider the toxicity of nanomaterials, and their size, shape, solubility, composition, and crystallization should be evaluated to increase their biocompatibility. The chirality-induced differential biological effects should be taken into account as well, which may have an obvious effect on biotoxicity, biocompatibility, and biological functions. Based on the specific chirality-induced biological effects, chiral inorganic nanomaterials with multiple functional properties have been widely used in enantiomeric discrimination, chiral catalysis, biosensing, and biomedical treatment.

4.1 Enantiomeric discrimination

Enantiomeric discrimination is of great importance in biological chemistry and pharmacy. Numerous techniques based on chiral inorganic nanostructures have been developed to discriminate or separate racemic medicines and compounds, taking advantage of the specific surficial, configurational, chemical, optical, electrical, and magnetic properties, especially the different affinities between chiral inorganic nanomaterials and chiral molecules.

Sun *et al.* used Cys-modified gold NPs to identify tyrosine (Tyr) or Phe enantiomers. When the chiral configuration of Tyr or Phe was identical to that of Cys, the obtained Raman scattering signals were several times stronger than those with the opposite chirality,[70] allowing for widespread application of chirality-related detection with high specificity and sensitivity. It was observed that β-cyclodextrin-modified silver NPs aggregated in the presence of L-Tyr due to the preferential recognition with L-Tyr,[71] which resulted in the signal simplification of pulse voltammograms and can be used for chiral discrimination of tyrosine enantiomers. In a recent study, Cys- or penicillamine (Pen)-modified gold NPs showed excellent discrimination ability for racemic propylene oxide, with Pen-modified gold NPs showing much higher recognition efficiency.[72] Additionally, L-Cys-capped CdTe QDs were used as chiral probes to recognize and quantify Tyr enantiomers using fluorescence and CD signals.[73]

4.2 Chiral catalysis

Artificial enzymes with chiral catalytic ability have been widely developed due to their excellent performance in pharmacy, biological transformation, and regulation of physical activities.[74] Chiral inorganic nanomaterials possess the ability to bio-mimic catalysis, which could be utilized to overcome the limitations of natural enzymes, such as poor extraction economy, low structural and activity stability, and severe difficulties in reutilization.

L-/D-Phe-stabilized cerium oxide NPs exhibited excellent stereoselectivity during the oxidation of dihydroxyphenylalanine (DOPA) enantiomers. In detail, the ability of L-Phe-modified cerium oxide NPs to catalyze the oxidation of D-DOPA was higher, and similarly, the efficiency of D-Phe cerium oxide NPs in the catalysis of L-DOPA was also higher.[75] Mesoporous silica NPs loaded with Cys-modified gold NPs showed high enantioselectivity for L-/D-3,4-DOPA.[76] In these cases, inorganic cores acted as the active catalytic center, and the chiral ligands on the surface served as recognition sites. Random-coiled DNA molecules and multi-stranded DNA can be switched under external stimulation (Fig. 5).

Ding *et al.* used DNA as environmental-responsive chiral ligands to modify gold NPs and construct glucose oxidase-like nanocatalysts. DNA molecules on the surface of gold NPs can provide the capability for the stereoselectivity of glucose enantiomers. Randomly coiled DNA-modified gold NPs preferentially catalyzed the oxidation of L-glucose. In contrast, structured DNA-capped gold NPs exhibited higher activity against D-glucose. Moreover, the ligand and substrate chirality-dependent size enlargement of gold NPs was also achieved by self-catalytic Au^0 deposition.[77] L-Pen-stabilized $Cu_{2-x}S$ QDs with enantioselective catalysis exhibited high ability to degrade BSA under excitation of left CPL, which was attributed to the excellent binding affinity and strong photon absorption ability.[78] Additionally, Cys-modified CdTe QDs were able to recognize DNA sequences at specific sites and cleave DNA molecules under CPL excitation, mimicking a restriction endonuclease.[79] However, the high toxicity of CdTe continues to limit its extensive and practical application. In addition to chiral NPs, chiral supraparticles (SPs) are desirable as chiral catalysts due to their more optimal enantioselectivity and catalytic ability. For example, chiral ZnS SPs with 3D chiral internal pores can act as photocatalysts for the enantioselective conversion of L-/D-Tyr to dityrosine.[80] Compared with chiral ZnS NPs, the enantioselectivity and catalytic ability of ZnS SPs enhanced obviously.

4.3 Biosensing

CD signals of biological molecules are usually distributed in the UV range, while the CD signals of inorganic nanomaterials can be regulated to the visible or NIR. Therefore, the CD signals of inorganic nanomaterials will not be disturbed by biological systems and can be used as sensing signals in biological systems. The *g*-factor values of inorganic nanomaterials can also be highly enhanced by plasmonic coupling, electron hybridization, and atomic distortion of the surface crystal lattice, which will enhance the sensitivity of detection.

There has been significant progress in the use of chiral inorganic nanomaterials with specific morphologies and optical activities for the ultrasensitive detection of biomarkers.[8] For example, S. Li *et al.* developed DNA-driven gold-upconversion nanopyramids with strong CD and luminescence signals. Caused by the competitive recognition in the presence of microRNA21, the CD signal of nanopyramids decreased, while the luminescence signal recovered due to the dissociation of nanopyramids.[63] Because of their excellent biocompatibility and biostability obtained after specific modifications, nanopyramids are suitable for *in situ* cancer cell detection. Ultrathin CdSe NPLs modified with L-/D-Cys can be used as ultrasensitive probes for sensing lead ions. In the presence of lead ions, the amount of Cys on the surface of CdSe NPLs decreases due to Pb–S bonding, leading to decreased CD intensity.[55]

Ngamdee *et al.* reported a glucose detection method based on Cys and D-Pen co-modified CdS QDs. Chiral CdS

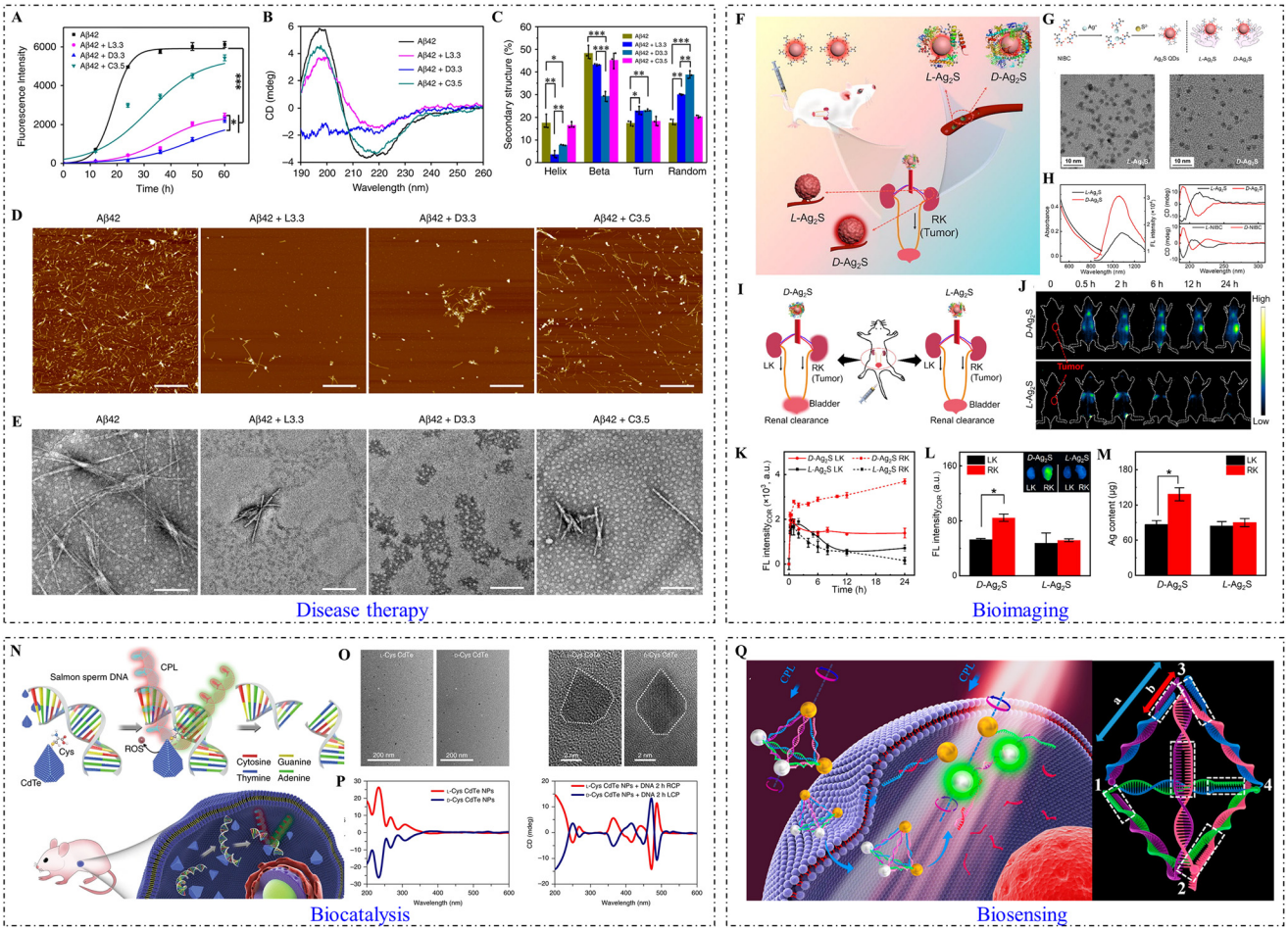

Fig. 5 Biological applications of inorganic chiral NPs. (A) ThT fluorescence assay of Aβ42 peptide in the absence and presence of Aβ42 + L3.3, Aβ42 + D3.3, or Aβ42 + C3.5. (B) CD spectra of Aβ42 in the absence and presence of L3.3, D3.3, or C3.5 after co-incubation for 48 h. (C) Analysis of protein secondary structure. (D) AFM images and (E) TEM images of Aβ42 in the absence and presence of L3.3, D3.3, or C3.5 after co-incubation for 48 h (from left to right). (Aβ42 + L3.3: 3.3 nm L-GSH-capped gold NPs; Aβ42 + D3.3: 3.3 nm D-GSH-capped gold NPs; Aβ42 + C3.5: 3.5 nm citrate-capped gold NPs).[84] Reproduced from ref. 84 with permission from Nature Publishing Group, copyright 2020. (F) Scheme of *in vivo* biological interactions. (G) Schematic illustration of chiral Ag_2S QD synthetic strategy (top) and TEM images of L-Ag_2S QDs and D-Ag_2S QDs (bottom: from left to right). (H) The UV–Vis absorption and emission spectra of L-Ag_2S QDs and D-Ag_2S QDs (left), and CD spectra of L-/D-Ag_2S QDs and their corresponding ligands (L-/D-NIBC) (right: from top to bottom). (I) Schematic illustration of the transport of Ag_2S QDs in an orthotopic kidney tumor mouse model. (J) *In vivo* NIR-II fluorescence images of mice intravenously injected with L-/D-Ag_2S QDs at different periods. (K) Plots of the fluorescence intensity of LK and RK *versus* time. (L) *Ex vivo* images of dissected kidneys and their fluorescence intensity. (M) Silver content analysis of the dissected kidneys. (LK: normal kidney tumor model; RK: orthotopic kidney tumor model).[56] Reproduced from ref. 56 with permission from Elsevier, copyright 2022. (N) Strategy for site-selective DNA cleavage by chiral CdTe NPs. (O) TEM (left) and high-resolution TEM (right) images of truncated tetrahedron-shaped L-Cys and D-Cys CdTe NPs. (P) CD spectra of L-Cys and D-Cys CdTe NPs (left), and L-Cys and D-Cys CdTe NPs mixed with DNA and illuminated under 405 nm RCP/LCP for 2 h (right).[79] Reproduced from ref. 79 with permission from Nature Publishing Group, copyright 2018. (Q) Schematic illustration of gold-UCNP pyramids for miRNA detection (left) and the nucleic acid skeleton of a pyramid used for miRNA detection (right).[63] Reproduced from ref. 63 with permission from the American Chemistry Society, copyright 2016.

QDs can be disrupted by H_2O_2 generated from glucose oxidation, which leads to a decrease in CD signals. Therefore, chiral CdS QDs can be used to detect glucose.[81] Additionally, Liz-Marzán *et al.* used CD signals in the NIR range to detect amyloid fibrils in Parkinson's disease, and thus there is great potential for their use in the detection of neurodegenerative diseases.[45] In a recent study, C. Li *et al.* synthesized aspartate-coated $Co(OH)_2$ NPs with unique magnetic properties, strong chiral signals, and low biotoxicity, and they were used to detect reactive oxygen species (ROS) in living cells with high sensitivity. In the presence of ROS, Co^{2+} oxidation on the surface of NPs occurs and results in significant decreases in CD signal and obvious change in the magnetic resonance imaging (MRI) ability. Therefore, CD signals and MRI can be used to detect ROS with high selectivity and sensitivity.[82]

4.4 Diagnosis and treatment of diseases

Chiral inorganic nanomaterials have been widely used in the diagnosis and treatment of diseases because of their multiple

functions of biomimicking catalytic ability and photon thermal/dynamic therapy capabilities.[83,84]

C. Xu's team synthesized chiral gold NPs with a helical configuration that activated apoptosis for senescent microglia under NIR excitation at 808 nm without harming normal cells. This method offers new possibilities for treating Parkinson's disease with high specificity and selectivity.[85] Yan *et al.* found that D-Cys-modified gold NPs exhibited stronger antibacterial ability with lower disturbance of the balance of intestinal bacterial colonies compared with L-Cys-modified gold NPs.[86] Chiral inorganic nanomaterials can also be used for disease therapy.

Recently, Y. M. Wang *et al.* developed pH/H_2O_2-responsive probes using chiral mesoporous silica NRs with drugs loading inside, which were able to release drugs at the tumor site with high responsiveness.[87] Y. Liu *et al.* synthesized L-/D-Pen-modified $Cu_{2-x}Se$ NPs that were able to synergistically participate in chemodynamic therapy (CDT) and photothermal therapy (PTT) cancer treatments under secondary NIR light irradiation. Furthermore, there was higher treatment efficacy with D-Pen-modified $Cu_{2-x}Se$ NPs as compared to L-Pen-modified $Cu_{2-x}Se$ NPs.[88]

T. Liu *et al.* reported the use of glutamine and lysine co-modified gold NPs as photothermal agents for tumor elimination. After uptake by cancer cells, intracellular assembly of gold NPs occurred due to the polymerization of glutamine and lysine catalyzed by intracellular transglutaminase, thus providing excellent photothermal ability for precise tumor treatment.[89] Moreover, Y. Li *et al.* synthesized chiral MoO_{3-x} NPs *via* step-by-step reduction treatment using Cys enantiomers as chiral ligands, which can be used as photothermal agents to eliminate tumor cells under the photon irradiation of NIR light. The highest mortality of HeLa cells was obtained with L-Cys-MoO_{3-x} NPs under the excitation of L-CPL, and *vice versa* for D-Cys-MoO_{3-x} with D-CPL.[90]

5. Summary and outlook

Due to the specific biological effects and multi-functional properties of chiral inorganic nanomaterials, they have largely spurred the research areas of disease therapeutics, drug carriers, medical imaging, physiological diagnosis, biological cytology, pharmaceutical preparation and separation, and biometric identification. However, many problems remain to be solved when considering further development and application. First, many chiral inorganic nanomaterials are constructed with strong chiral optical activities, but because the chiral origin of some chiral materials remains unclear, exploration of the origins of chirality is necessary. Second, *in vivo* studies have mainly been conducted with animals, which creates a particular gap between animals and human bodies. Thus, there is an immediate need for clinical research on these synthesized materials. Third, accumulation of nanomaterials can lead to biotoxicity, which is mainly related to the particle size, chiral ligands, and inherent toxicity of inorganic cores. Even though the toxicity can be reduced by chiral induction and surface modification, a lack of biocompatibility continues to exist in some specific biological environments.

It is necessary to conduct in-depth research on chiral inorganic nanomaterials and expand new methods to solve biologically related problems based on multidisciplinary intersections and new technologies. This review will guide the development of chiral inorganic nanomaterials with excellent biological functionalities and provide new tools to solve biologically related problems.

Conflicts of interest

There are no conflicts to declare.

Acknowledgements

This work was supported by the National Natural Science Foundation of China (32101142), the National Natural Science Foundation of Jiangsu Province (BK20221532), and the Fundamental Research Funds for the Central Universities (JUSRP622037).

References

1 W. Ma, L. G. Xu, A. F. de Moura, X. L. Wu, H. Kuang, C. L. Xu and N. A. Kotov, *Chem. Rev.*, 2017, **117**, 8041–8093.
2 F. Devínsky, *Symmetry*, 2021, **13**, 2277.
3 R. Espinosa-Cardenas, A. Arce-Sillas, D. Alvarez-Luquin, J. Leyva-Hernandez, E. Montes-Moratilla, I. Gonzalez-Saavedra, M. C. Boll, E. Garcia-Garcia, S. Angeles-Perea, G. Fragoso, E. Sciutto and L. Adalid-Peralta, *J. Neuroimmunol.*, 2020, **347**, 577328.
4 P. Adhikari, B. Xie, A. Semeano, A. Bonifazi, F. O. Battiti, A. H. Newman, H. Yano and L. Shi, *Biomolecules*, 2021, **11**, 570.
5 X. L. Zhao, S. Q. Zang and X. Y. Chen, *Chem. Soc. Rev.*, 2020, **49**, 2481–2503.
6 P. Slepicka, N. S. Kasalkova, J. Siegel, Z. Kolska and V. Svorcik, *Materials*, 2020, **13**, 1.
7 J. J. Liu, L. Yang, P. Qin, S. Q. Zhang, K. K. L. Yung and Z. F. Huang, *Adv. Mater.*, 2021, **33**, 2005506.
8 Y. N. Shao, G. L. Yang, J. Y. Lin, X. F. Fan, Y. Guo, W. T. Zhu, Y. Cai, H. Y. Huang, D. Hu, W. Pang, Y. J. Liu, Y. W. Li, J. J. Cheng and X. Q. Xu, *Theranostics*, 2021, **11**, 9262–9295.
9 L. Xiao, T. T. An, L. Wang, X. L. Xu and H. D. Sun, *Nano Today*, 2020, **30**, 100824.
10 N. Abid, M. Khan, S. Shujait, K. Chaudhary, M. Ikram, M. Imran, J. Haider, M. Khan, Q. Khan and M. Maqbool, *Adv. Colloid Interface Sci.*, 2022, **300**, 102597.

11 M. J. Urban, C. Shen, X. T. Kong, C. Zhu, A. O. Govorov, Q. Wang, M. Hentschel and N. Liu, *Annu. Rev. Phys. Chem.*, 2019, **70**, 275–299.
12 H. Kim, K. M. Bang, H. Ha, N. H. Cho, S. D. Namgung, S. W. Im, K. H. Cho, R. M. Kim, W. I. Choi, Y. C. Lim, J. Y. Shin, H. K. Song, N. K. Kim and K. T. Nam, *ACS Nano*, 2021, **15**, 979–988.
13 J. Yeom, U. S. Santos, M. Chekini, M. Cha, A. F. de Moura and N. A. Kotov, *Science*, 2018, **359**, 309–314.
14 H. Huang, L. L. Hu, Y. Sun, Y. Liu, Z. H. Kang and D. R. MacFarlane, *Microchim. Acta*, 2019, **186**, 2–9.
15 S. Jiang, M. Chekini, Z. B. Qu, Y. C. Wang, A. Yeltik, Y. G. Liu, A. Kotlyar, T. Y. Zhang, B. Li, H. V. Demir and N. A. Kotov, *J. Am. Chem. Soc.*, 2017, **139**, 13701–13712.
16 J. Luo, Y. Cheng, Z. W. Gong, K. Wu, Y. Zhou, H. X. Chen, M. Gauthier, Y. Z. Cheng, J. Liang and T. Zou, *Langmuir*, 2020, **36**, 600–608.
17 H. E. Lee, H. Y. Ahn, J. Mun, Y. Y. Lee, M. Kim, N. H. Cho, K. Chang, W. S. Kim, J. Rho and K. T. Nam, *Nature*, 2018, **556**, 360–365.
18 H. Kim, S. W. Im, N. H. Cho, D. H. Seo, R. M. Kim, Y. C. Lim, H. E. Lee, H. Y. Ahn and K. T. Nam, *Angew. Chem., Int. Ed.*, 2020, **59**, 12976–12983.
19 X. Wen, S. Wang, R. L. Liu, R. Duan, S. Hu, T. F. Jiao, L. Zhang and M. H. Liu, *Small*, 2022, **18**, 2104301.
20 S. Wang, L. H. Zheng, W. J. Chen, L. K. Ji, L. Zhang, W. S. Lu, Z. Y. Fang, F. C. Guo, L. M. Qi and M. H. Liu, *CCS Chem.*, 2021, **2**, 2473–2484.
21 S. Li, L. W. Xu, M. R. Lu, M. Z. Sun, L. G. Xu, C. L. Hao, X. L. Wu, C. L. Xu and H. Kuang, *Nano Res.*, 2021, **14**, 2451–2455.
22 F. Purcell-Milton, R. McKenna, L. J. Brennan, C. P. Cullen, L. Guillemeney, N. V. Tepliakov, A. S. Baimuratov, I. D. Rukhlenko, T. S. Perova, G. S. Duesberg, A. V. Baranov, A. V. Fedorov and Y. K. Gun'ko, *ACS Nano*, 2018, **12**, 954–964.
23 J. Morales-Vidal, N. Lopez and M. A. Ortuno, *J. Phys. Chem. C*, 2019, **123**, 13758–13764.
24 P. Rodríguez-Zamora, B. Salazar-Angeles, F. Buendia, C. Cordero-Silis, J. Fabila, L. Bazan-Diaz, L. M. Fernandez-Diaz, L. O. Paz-Borbon, G. Diaz and I. L. Garzon, *J. Raman Spectrosc.*, 2020, **51**, 243–255.
25 G. M. Li, X. N. Fei, H. F. Liu, J. Gao, J. Y. Nie, Y. B. Wang, Z. D. Tian, C. C. He, J. L. Wang, C. Ji, D. Oron and G. L. Yang, *ACS Nano*, 2020, **14**, 4196–4205.
26 V. A. Kuznetsova, E. Mates-Torres, N. Prochukhan, M. Marcaste, F. Purcell-Milton, J. O'Brien, A. K. Visheratina, M. Martinez-Carmona, Y. Grornova, M. Garcia-Melchor and Y. K. Gun'ko, *ACS Nano*, 2019, **13**, 13560–13572.
27 X. J. Mu, J. G. Wang, G. Q. Duan, Z. J. Li, J. X. Wen and M. T. Sun, *Spectrochim. Acta, Part A*, 2019, **212**, 188–198.
28 W. Ma, L. G. Xu, L. B. Wang, C. L. Xu and H. Kuang, *Adv. Funct. Mater.*, 2019, **29**, 1805512.
29 A. Visheratina and N. A. Kotov, *CCS Chem.*, 2020, **2**, 583–604.
30 S. Mokashi-Punekar, Y. C. Zhou, S. C. Brooks and N. L. Rosi, *Adv. Mater.*, 2020, **32**, 1905975.
31 N. V. Karimova and C. M. Aikens, *Part. Part. Syst. Charact.*, 2019, **36**, 1900043.
32 A. Kuzyk, R. Schreiber, Z. Y. Fan, G. Pardatscher, E. M. Roller, A. Hogele, F. C. Simmel, A. O. Govorov and T. Liedl, *Nature*, 2012, **483**, 311–314.
33 S. Mokashi-Punekar, S. C. Brooks, C. D. Hogan and N. L. Rosi, *Biochemistry*, 2021, **60**, 1044–1049.
34 W. Heyvaert, A. Pedrazo-Tardajos, A. Kadu, N. Claes, G. Gonzalez-Rubio, L. M. Liz-Marzan, W. Albrecht and S. Bals, *ACS Mater. Lett.*, 2022, **4**, 642–649.
35 J. J. Cheng, G. Le Saux, J. Gao, T. Buffeteau, Y. Battie, P. Barois, V. Ponsinet, M. H. Delville, O. Ersen, E. Pouget and R. Oda, *ACS Nano*, 2017, **11**, 3806–3818.
36 W. J. Yan, L. G. Xu, C. L. Xu, W. Ma, H. Kuang, L. B. Wang and N. A. Kotov, *J. Am. Chem. Soc.*, 2012, **134**, 15114–15121.
37 G. Gonzalez-Rubio, J. Mosquera, V. Kumar, A. Pedrazo-Tardajos, P. Llombart, D. M. Solis, I. Lobato, E. G. Noya, A. Guerrero-Martinez, J. M. Taboada, F. Obelleiro, L. G. MacDowell, S. Bals and L. M. Liz-Marzan, *Science*, 2020, **368**, 1472–1477.
38 J. Yan, W. C. Fang, J. Y. Kim, J. Lu, P. Kumar, Z. Z. Mu, X. C. Wu, X. M. Mao and N. A. Kotov, *Chem. Mater.*, 2020, **32**, 476–488.
39 J. S. Kang, N. Kim, T. Kim, M. Seo and B. S. Kim, *Macromol. Rapid Commun.*, 2022, **43**, 2100649.
40 K. Saito and T. Tatsuma, *Nano Lett.*, 2018, **18**, 3209–3212.
41 J. Y. Kim, J. Yeom, G. P. Zhao, H. Calcaterra, J. Munn, P. J. Zhang and N. Kotov, *J. Am. Chem. Soc.*, 2019, **141**, 11739–11744.
42 H. Wang, Y. Liu, J. Yu, Y. Luo, L. Wang, T. Yang, B. Raktani and H. Lee, *ACS Appl. Mater. Interfaces*, 2022, **14**, 3559–3567.
43 R. Nizam and A. Zafar, *Int. J. Eng. Appl. Sci. Technol.*, 2019, **4**, 175–179.
44 T. T. Zhuang, Y. Li, X. Q. Gao, M. Y. Wei, F. P. G. de Arquer, P. Todorovic, J. Tian, G. P. Li, C. Zhang, X. Y. Li, L. Dong, Y. H. Song, Y. Lu, X. K. Yang, L. B. Zhang, F. J. Fan, S. O. Kelley, S. H. Yu, Z. Y. Tang and E. H. Sargent, *Nat. Nanotechnol.*, 2020, **15**, 192–197.
45 J. Kumar, H. Erana, E. Lopez-Martinez, N. Claes, V. F. Martin, D. M. Solis, S. Bals, A. L. Cortajarena, J. Castilla and L. M. Liz-Marzán, *Proc. Natl. Acad. Sci. U. S. A.*, 2018, **115**, 3225–3230.
46 Q. F. Zhang, T. Hernandez, K. W. Smith, S. A. H. Jebeli, A. X. Dai, L. Warning, R. Baiyasi, L. A. McCarthy, H. Guo, D. H. Chen, J. A. Dionne, C. F. Landes and S. Link, *Science*, 2019, **365**, 1475–1478.
47 F. L. Gao, M. Z. Sun, W. Ma, X. L. Wu, L. Q. Liu, H. Kuang and C. L. Xu, *Adv. Mater.*, 2017, **29**, 1606864.
48 L. Nguyen, M. Dass, M. F. Ober, L. V. Besteiro, Z. M. M. Wang, B. Nickel, A. O. Govorov, T. Liedl and A. Heuer-Jungemann, *ACS Nano*, 2020, **14**, 7454–7461.
49 X. Lan, T. J. Liu, Z. M. Wang, A. O. Govorov, H. Yan and Y. Liu, *J. Am. Chem. Soc.*, 2018, **140**, 11763–11770.

50 A. H. Qu, M. Z. Sun, J. Y. Kim, L. G. Xu, C. L. Hao, W. Ma, X. L. Wu, X. G. Liu, H. Kuang, N. A. Kotov and C. L. Xu, *Nat. Biomed. Eng.*, 2021, **5**, 103–113.
51 L. G. Xu, X. X. Wang, W. W. Wang, M. Z. Sun, W. J. Choi, J. Y. Kim, C. L. Hao, S. Li, A. H. Qu, M. R. Lu, X. L. Wu, F. M. Colombari, W. R. Gomes, A. L. Blanco, A. F. de Moura, X. Guo, H. Kuang, N. A. Kotov and C. L. Xu, *Nature*, 2022, **601**, 366–373.
52 W. C. Feng, J. Y. Kim, X. Z. Wang, H. A. Calcaterra, Z. B. Qu, L. Meshi and N. A. Kotov, *Sci. Adv.*, 2017, **3**, 12.
53 J. J. Hao, F. H. Zhao, Q. S. Wang, J. Y. Lin, P. X. Chen, J. Z. Li, D. X. Zhang, M. J. Chen, P. Z. Liu, M. H. Delville, T. C. He, J. J. Cheng and Y. W. Li, *Adv. Opt. Mater.*, 2021, **9**, 2101142.
54 M. P. Moloney, J. Govan, A. Loudon, M. Mukhina and Y. K. Gun'ko, *Nat. Protoc.*, 2015, **10**, 558–573.
55 X. B. Wang, J. J. Hao, J. J. Cheng, J. Z. Li, J. Miao, R. X. Li, Y. W. Li, J. E. Li, Y. H. Liu, X. Zhu, Y. J. Liu, X. W. Sun, Z. K. Tang, M. H. Delville, T. C. He and R. Chen, *Nanoscale*, 2019, **11**, 9327–9334.
56 S. H. Qu, Q. Jia, Z. Li, Z. L. Wang and L. Shang, *Sci. Bull.*, 2022, **67**, 1274–1283.
57 Y. M. Wang, W. Li, T. T. Liu, L. Xu, Y. Y. Guo, J. Ke, S. M. Li and H. R. Li, *Mater. Sci. Eng., C*, 2019, **103**, 109737.
58 Q. Maqbool, A. Jung, S. Won, J. Cho, J. G. Son and B. Yeom, *ACS Appl. Mater. Interfaces*, 2021, **13**, 54301–54307.
59 W. Ma, J. T. Mao, C. L. Hao, L. G. Xu, C. L. Xu and H. Kuang, *Appl. Catal., B*, 2019, **245**, 691–697.
60 W. Ma, M. Z. Sun, P. Fu, S. Li, L. G. Xu, H. Kuang and C. L. Xu, *Adv. Mater.*, 2017, **29**, 1703410.
61 M. Z. Sun, T. T. Hao, X. Y. Li, A. H. Qu, L. G. Xu, C. L. Hao, C. L. Xu and H. Kuang, *Nat. Commun.*, 2018, **9**, 4494.
62 C. M. Walters, K. R. Adair, W. Y. Hamad and M. J. MacLachlan, *Eur. J. Inorg. Chem.*, 2020, **2020**, 3937–3943.
63 S. Li, L. G. Xu, W. Ma, X. L. Wu, M. Z. Sun, H. Kuang, L. B. Wang, N. A. Kotov and C. L. Xu, *J. Am. Chem. Soc.*, 2016, **138**, 306–312.
64 X. Shao, T. Y. Zhang, B. Li, M. H. Zhou, X. Y. Ma, J. C. Wang and S. Jiang, *Inorg. Chem.*, 2019, **58**, 6534–6543.
65 L. Yang, P. Nandi, Y. C. Ma, J. J. Liu, U. Mirsaidov and Z. F. Huang, *Small*, 2020, **16**, 1906048.
66 M. Matuschek, D. P. Singh, H. H. Jeong, M. Nesterov, T. Weiss, P. Fischer, F. Neubrech and N. Liu, *Small*, 2018, **14**, 1702990.
67 H. L. Liu, Z. Li, Y. Yan, J. Q. Zhao and Y. Wang, *Nanoscale*, 2019, **11**, 21990–21998.
68 K. J. Jeong, D. K. Lee, V. Tran, C. F. Wang, J. W. Lv, J. Park, Z. Y. Tang and J. Lee, *ACS Nano*, 2020, **14**, 7152–7160.
69 F. Albalawi, M. Z. Hussein, S. Fakurazi and M. J. Masarudin, *Int. J. Nanomed.*, 2021, **16**, 161–184.
70 X. P. Sun, N. Wang, Y. X. He, H. J. Kong, H. F. Yang and X. L. Liu, *J. Mater. Chem. B*, 2021, **9**, 7167–7171.
71 S. S. Wu, H. Wang, D. T. Wu, G. C. Fan, Y. X. Tao and Y. Kong, *Analyst*, 2021, **146**, 1612–1619.
72 N. Shukla, Z. Blonder and A. J. Gellman, *Nanomaterials*, 2020, **10**, 8.
73 F. Feizi, M. Shamsipur, A. Barati, M. B. Gholivand and F. Mousavi, *Microchem. J.*, 2020, **158**, 105168.
74 R. F. Zhang, Y. L. Zhou, X. Y. Yan and K. L. Fan, *Microchim. Acta*, 2019, **186**, 782.
75 Y. H. Sun, C. Q. Zhao, N. Gao, J. S. Ren and X. G. Qu, *Chem. – Eur. J.*, 2017, **23**, 18146–18150.
76 Y. Zhou, H. J. Sun, H. C. Xu, S. Matysiak, J. S. Ren and X. G. Qu, *Angew. Chem., Int. Ed.*, 2018, **57**, 16791–16795.
77 P. F. Zhan, Z. G. Wang, N. Li and B. Q. Ding, *ACS Catal.*, 2015, **5**, 1489–1498.
78 C. L. Hao, R. Gao, Y. Li, L. G. Xu, M. Z. Sun, C. L. Xu and H. Kuang, *Angew. Chem., Int. Ed.*, 2019, **58**, 7371–7374.
79 M. Z. Sun, L. G. Xu, A. H. Qu, P. Zhao, T. T. Hao, W. Ma, C. L. Hao, X. D. Wen, F. M. Colombari, A. F. de Moura, N. A. Kotov, C. L. Xu and H. Kuang, *Nat. Chem.*, 2018, **10**, 821–830.
80 S. Li, J. Liu, N. S. Ramesar, H. Heinz, L. G. Xu, C. L. Xu and N. A. Kotov, *Nat. Commun.*, 2019, **10**, 4826.
81 K. Ngamdee and W. Ngeontae, *Sens. Actuators, B*, 2018, **274**, 402–411.
82 C. Li, S. Li, J. Zhao, M. Z. Sun, W. W. Wang, M. R. Lu, A. H. Qu, C. L. Hao, C. Chen, C. L. Xu, H. Kuang and L. G. Xu, *J. Am. Chem. Soc.*, 2022, **144**, 1580–1588.
83 Y. Wen, M. Q. He, Y. L. Yu and J. H. Wang, *Adv. Colloid Interface Sci.*, 2021, **289**, 102376.
84 K. Hou, J. Zhao, H. Wang, B. Li, K. X. Li, X. H. Shi, K. W. Wan, J. Ai, J. W. Lv, D. W. Wang, Q. X. Huang, H. Y. Wang, Q. Cao, S. Q. Liu and Z. Y. Tang, *Nat. Commun.*, 2020, **11**, 4790.
85 Z. J. Xu, A. H. Qu, H. Y. Zhang, W. W. Wang, C. L. Hao, M. R. Lu, B. M. Shi, L. G. Xu, M. Z. Sun, C. L. Xu and H. Kuang, *Chem. Sci.*, 2022, **13**, 6642–6654.
86 Y. L. Xu, H. X. Wang, M. Zhang, J. H. Zhang and W. J. Yan, *Nanomaterials*, 2021, **11**, 1621.
87 Y. M. Wang, J. Wang, K. J. Gou, W. Kang, X. M. Guo, K. Y. Zhu, S. M. Li and H. R. Li, *ACS Appl. Mater. Interfaces*, 2021, **13**, 35397–35409.
88 Y. F. Liu, H. M. Li, S. L. Li, X. Y. Zhang, J. Q. Xiong, F. L. Jiang, Y. Liu and P. Jiang, *ACS Appl. Mater. Interfaces*, 2021, **13**, 60933–60944.
89 T. Liu, R. H. Jin, P. Y. Yuan, Y. K. Bai, B. L. Cai and X. Chen, *ACS Appl. Mater. Interfaces*, 2019, **11**, 28621–28630.
90 Y. W. Li, Z. W. Miao, Z. W. Shang, Y. Cai, J. J. Cheng and X. Q. Xu, *Adv. Funct. Mater.*, 2020, **30**, 1906311.

